Steel and Composite Structures, *Vol. 32, No. 6 (2019) 701-715*
DOI: https://doi.org/10.12989/scs.2019.32.6.701

Creep damage and life assessment of thick cylindrical pressure vessels with variable thickness made of 304L austenitic stainless steel

Mosayeb Davoudi Kashkoli [1a], Khosro Naderan Tahan [1b] and Mohammad Zamani Nejad [*2]

[1] *Department of Mechanical Engineering, Shahid Chamran University of Ahvaz, Ahvaz, Iran*
[2] *Department of Mechanical Engineering, Yasouj University, Yasouj, Iran*

(*Received August 4, 2018, Revised August 12, 2019, Accepted September 7, 2019*)

Abstract. Using first-order shear deformation theory (FSDT), a semi-analytical solution is employed to analyze creep damage and remaining life assessment of 304L austenitic stainless steel thick (304L ASS) cylindrical pressure vessels with variable thickness subjected to the temperature gradient and internal non-uniform pressure. Damages are obtained in thick cylinder using Robinson's linear life fraction damage rule, and time to rupture and remaining life assessment is determined by Larson-Miller Parameter (LMP). The thermo-elastic creep response of the material is described by Norton's law. The novelty of the present work is that it seeks to investigate creep damage and life assessment of the vessels with variable thickness made of 304L ASS using LMP based on first-order shear deformation theory. A numerical solution using finite element method (FEM) is also presented and good agreement is found. It is shown that temperature gradient and non-uniform pressure have significant influences on the creep damages and remaining life of the vessel.

Keywords: 304L austenitic stainless steel (304L ASS); creep damage; life assessment; cylindrical pressure vessels; first-order shear deformation theory

1. Introduction

Cylindrical vessels are often used as the basic process component in various structural and engineering applications such as nuclear, aircraft, gun barrels, space engineering, oil-transmitting pipeline, power generation equipments and pressure vessels (Ghannad *et al*. 2009, Nejad and Rahimi 2009a, b, Fatehi and Nejad 2014, Nejad *et al*. 2014, 2015c, 2016, 2018a, b, Nejad and Hadi 2016a, b, Singh and Gupta 2014, Afshin *et al*. 2017, Gharibi *et al*. 2017, Kashkoli and Nejad 2014, 2015, 2018). Under high thermo-mechanical loadings, the life of these components reduce due to the creep phenomenon occurs (Khanna *et al*. 2017). Creep is the time-dependent plastic deformation which occurs when a material is subjected to a constant stress/load and operating at elevated temperatures for a long time, which may lead to catastrophic failure (Valluri *et al*. 2010). Therefore, the analysis of creep deformations and prediction of strain rates and fracture time is very important in these applications. Creep of metals and ceramics occurs over three broad temperature ranges: high ($T > 0.6T_m$, melting point), intermediate ($0.3T_m < T < 0.6T_m$), and low ($T < 0.3T_m$) (Kassner *et al*. 2015). This paper concerns itself largely with the intermediate temperature range. Using the shells with variable thickness is one of the ways to optimize the shells weight and also stress distribution (Ghannad *et al*. 2013). Although the literature on the creep stresses of these shells are quite limited. Shear deformation theory is very suitable method for the purpose of calculation of stresses and displacements in axisymmetric thick shells, plates and beams (Sofiyev and Osmancelebioglu 2017, Sofiyev 2017, 2018a, b, Ghannad *et al*. 2012, Nejad *et al*. 2015a, b, 2017a, b, c, d, Abdelaziz *et al*. 2017, Jandaghian and Rahmani 2017, Mahmoud 2017, Sekkal *et al*. 2017, Li and Hu 2016, Li *et al*. 2015, 2016, Hadi *et al*. 2018a, b, Simsek 2016, Nejad and Hadi 2016a, b, Kashkoli *et al*. 2018). This kind of structures, with different geometries, different loadings and different boundary conditions, with even variable pressure, could be more easily solved by this method (Ghannad *et al*. 2013). Elastic and thermo-elastic stresses in thick cylindrical shells made of homogeneous and functionally graded materials (FGMs) under thermal loading have been analyzed extensively in the past years (Dehghan *et al*. 2016, Ghannad and Nejad 2010, Jabbari *et al*. 2015, 2016, Kashkoli *et al*. 2017a, b, Mazarei *et al*. 2016, Nejad and Fatehi 2015, Nejad *et al*. 2009, 2017a, b, c, d, Dung and Dong 2016). The material constitutive models are important in creep analysis. Numerous models have been proposed to describe the primary and secondary creep stages (Kobelev 2014, Naumenko and Altenbach 2007, Yao *et al*. 2007). Among them, the most widespread creep constitutive models are the Bailey-Norton and Norton laws. Norton law has been used to obtain history of stresses and strains in pressure vessels by many researchers (Kashkoli *et al*. 2017a, b, Loghman and Wahab 1996, Loghman *et al*. 2010, 2012, Nejad and Kashkoli 2014, You *et al*. 2007, Yang 2000). The other creep models that are very used by

∗Corresponding author, Ph.D., Associate Professor,
E-mail: m_zamani@yu.ac.ir; m.zamani.n@gmail.com
[a] Ph.D.
[b] Ph.D., Professor

http://www.techno-press.org/?journal=scs&subpage=6
ISSN: 1229-9367 (Print), 1598-6233 (Online)

researchers are based on threshold stress and Seth's transition theory (Singh and Gupta 2010, 2011, 2012). Design procedures and residual life assessments for many components such as boiler tubes that are subjected to high temperature and stress conditions over a long time, require the accounting for creep and damage processes (Altenbach *et al*. 2008). Over the years the simple Robinson's linear life-fraction rule (Robinson 1952) has been very useful in estimating creep life under non-steady conditions of stress and/or temperature. Many researchers have worked on creep data extrapolation and several relationships have been suggested to correlate the creep test data. Among the proposed relationships, Larson–Miller parameter (LMP) is used widely for its simplicity (Viswanathan 1989). Larson and Miller introduced a grouping concept between temperature (T) and fracture time (t_r) of the creep test for a specific test stress (Viswanathan, 1989). Based on Larson–Miller grouping parameter, T and t_r of different creep tests can be related to each other when the stress level remains constant (Tahami *et al*. 2010). Therefore, when the creep fracture time under specific temperature is known, the LMP can be used to estimate the fracture time at a different temperature but under the same working stress. 304L ASS is being used in this paper as material due to its high strength, ductility and good corrosion and creep resistance (Wang *et al*. 2016, Carroll *et al*. 2016). Over the last years, hot deformation behavior of 304L ASS has been studied by many authors (Samantaray *et al*. 2016, Lopez and Zhang 2014, Taylor *et al*. 2011).

As mentioned above, to the best of the authors' knowledge, no analytical study has been carried out to date on creep response of cylindrical pressure vessels with variable thickness based on first-order shear deformation theory. In this study, assuming that the creep response of the material is governed by Norton's law, a semi-analytical solution is presented for the calculation of stresses and displacements of thick-walled cylindrical pressure vessels with variable thickness made of 304L austenitic stainless steel. The governing equations are based on first-order shear deformation theory that accounts for the transverse shear. The governing equations are derived, using minimum total potential energy principle. Robinson's linear life fraction damage rule has been used to predict the creep damage histories during the life of the cylinder and Larson-Miller Parameter (LMP) has been used to obtain creep remaining life assessment. The results obtained for stresses and displacements are validated using the finite element method (FEM). Good agreement is found between the results. Other assumptions considered in this paper are as follows:

- The structure is cylindrical and thick walled.
- The properties of the material are independent of temperature.
- The internal non uniform pressure distribution along the axis of the cylinder is nonlinear.

2. Basic formulation for thick walled cylinder

The process of formulation and obtaining the equations of creep displacements and stresses are as follows:

- Extracting the thermo-elastic governing equations (independent of time).
- Solving the thermo-elastic governing equations using eigenvectors and eigenvalues and disk form multilayer method.
- Applying boundary and continuity conditions (time independent).
- Extracting the creep governing equations using the Norton law.
- Solving the creep governing equations using eigenvectors and eigenvalues and disk form multilayer method.
- Applying boundary and continuity conditions (time dependent).
- Calculating the creep damage and life assessment of the cylinder using Robinson's linear life fraction damage rule and LMP, respectively.

A cross section of variable thickness clamp-clamp thick cylinder with length L, subjected to non-uniform internal pressure distribution P, and distributed temperature field due to a steady-state heat conduction is considered. The geometry, mechanical and thermal loadings and boundary conditions of the cylinder are shown in Fig. 1.

The location of an arbitrary point m in Fig. 1 is as follows

$$r = R + z \tag{1}$$

In Eq. (1), R is the middle surface radius and z represents the distance of the arbitrary point m from the middle surface.

In Eq. (1), the range of changes x and z are as follows

$$\begin{cases} 0 \leq x \leq L \\ -\dfrac{h}{2} \leq z \leq \dfrac{h}{2} \end{cases} \tag{2}$$

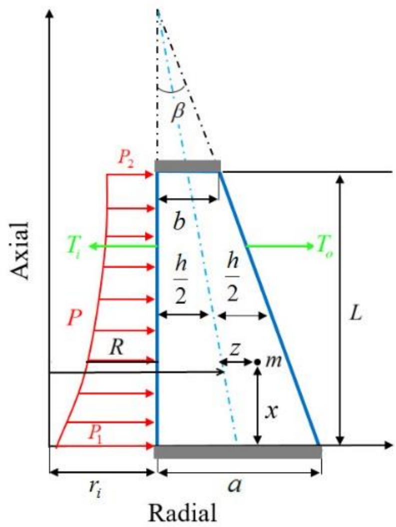

Fig. 1 Geometry, mechanical and thermal loadings and boundary conditions of the cylinder with variable thickness

In Eq. (1), the middle surface radius R and variable thickness h are as follows

$$\begin{cases} R = r_i + \frac{a}{2} - \frac{x}{2}(tan\,\beta) \\ h = a - x(tan\,\beta) \end{cases} \tag{3}$$

The vertex angle β is defined as

$$\beta = tan^{-1}\left[\frac{(a-b)}{L}\right] \tag{4}$$

The displacement field (U_x,U_θ,U_z) of the first order theory can be expressed in the form

$$\begin{cases} U_x(x,z) = u(x) + \phi(x)z \\ U_\theta(x,z) = 0 \\ U_z(x,z) = w(x) + \psi(x)z \end{cases} \tag{5}$$

where $u(x)$ and $w(x)$ denote the displacements of a point on the middle plane ($z = 0$) and $\phi(x)$ and $\psi(x)$ are the rotations of a transverse normal.

The strain–displacement relations in the cylindrical coordinate system are

$$\begin{cases} \varepsilon_x = \frac{\partial U_x}{\partial x} = \frac{du(x)}{dx} + \frac{d\phi(x)}{dx}z \\ \varepsilon_\theta = \frac{U_z}{r} = \frac{1}{R+z}(w(x) + \psi(x)z) \\ \varepsilon_z = \frac{\partial U_z}{\partial z} = \psi(x) \\ \gamma_{xz} = \frac{\partial U_x}{\partial z} + \frac{\partial U_z}{\partial x} = \phi(x) + \left(\frac{dw(x)}{dx} + \frac{d\psi(x)}{dx}z\right) \end{cases} \tag{6}$$

In addition, the thermal stresses based on constitutive equations for homogenous and isotropic materials are as follow

$$\begin{cases} \begin{Bmatrix} \sigma_x \\ \sigma_\theta \\ \sigma_z \end{Bmatrix} = \lambda E \begin{bmatrix} 1-\upsilon & \upsilon & \upsilon \\ \upsilon & 1-\upsilon & \upsilon \\ \upsilon & \upsilon & 1-\upsilon \end{bmatrix} \begin{Bmatrix} \varepsilon_x - \varepsilon_x^c \\ \varepsilon_\theta - \varepsilon_\theta^c \\ \varepsilon_z - \varepsilon_z^c \end{Bmatrix} \\ -\lambda E(1+\upsilon)\alpha_T T \begin{bmatrix} 1 \\ 1 \\ 1 \end{bmatrix} \\ \tau_{xz} = \lambda E\left(\frac{1-2\upsilon}{2}\right)\gamma_{xz} \\ \lambda = \frac{1}{(1+\upsilon)(1-2\upsilon)} \end{cases} \tag{7}$$

where T is temperature distribution and σ_i, ε_i and ε_i^c are, respectively, the stresses, strains and creep strains in the axial, circumferential and radial directions, also τ_{xz} and γ_{xz} are the shear stress and shear strain, respectively. υ, E and α_T are Poisson's ratio, modulus of elasticity and thermal expansion coefficient, respectively. The normal force (N_x,N_θ,N_z), bending moment (M_x,M_θ,M_z), shearing force (Q_x), and the twisting moment (M_{xz}) all in per unit length as terms of stress resultants are

$$\begin{cases} \{N_x, N_\theta, N_z\} = \int_{-\frac{h}{2}}^{\frac{h}{2}} \left\{\sigma_x\left(1+\frac{z}{R}\right), \sigma_\theta, \sigma_z\left(1+\frac{z}{R}\right)\right\} dz \\ \{M_x, M_\theta, M_z\} = \int_{-\frac{h}{2}}^{\frac{h}{2}} \left\{\sigma_x\left(1+\frac{z}{R}\right), \sigma_\theta, \sigma_z\left(1+\frac{z}{R}\right)\right\} zdz \\ Q_x = K\int_{-\frac{h}{2}}^{\frac{h}{2}} \tau_{xz}\left(1+\frac{z}{R}\right)dz \\ M_{xz} = K\int_{-\frac{h}{2}}^{\frac{h}{2}} \tau_{xz}\left(1+\frac{z}{R}\right)zdz \end{cases} \tag{8}$$

where K is the shear correction coefficient that is embedded in the shear stress term. In the static state, for cylindrical shells, $K = \frac{5}{6}$ (Jemielita 2002). The governing equations of the first-order shear deformation theory can be derived using the principle of virtual displacements (Jabbari *et al*. 2015)

$$\begin{cases} \frac{d}{dx}(RN_x) = 0 \\ \frac{d}{dx}(RM_x) - RQ_x = 0 \\ \frac{d}{dx}(RQ_x) - N_\theta = -P\left(R - \frac{h}{2}\right) \\ \frac{d}{dx}(RM_{xz}) - M_\theta - RN_z = P\frac{h}{2}\left(R - \frac{h}{2}\right) \end{cases} \tag{9}$$

and the boundary conditions at the two ends of the cylinder are

$$[R(N_x\delta u + M_x\delta\phi + Q_x\delta w + M_{xz}\delta\psi)]_0^L = 0 \tag{10}$$

The internal non uniform pressure distribution is selected as fallow

$$P = P_1 + (P_2 - P_1)\left(\frac{x}{L}\right)^{m_p} \tag{11}$$

Here P_1 and P_2 are the values of pressure at the $x = 0$ and $x = L$, respectively. m_p is constant parameter that is used to control the pressure profile. Substituting the stress components from Eq. (7) into Eq. (8) and then into the equilibrium Eq. (9), the following set of differential equation for displacement is obtained

$$\begin{cases} [B_1]\frac{d^2}{dx^2}\{y\} + [B_2]\frac{d}{dx}\{y\} + [B_3]\{y\} = \{F\} \\ \{y\} = \begin{Bmatrix} \frac{du(x)}{dx} & \phi(x) & w(x) & \psi(x) \end{Bmatrix}^T \end{cases} \tag{12}$$

where the coefficients matrices $[B_i]_{4\times4}$, and force vector $\{F\}_{4\times1}$ have been defined in the Appendix A.

2.1 Semi-analytical solution

Eq. (12) is the set of non-homogenous linear differential equations with variable coefficients. An analytical solution of this set of differential equations with variable coefficients seems to be difficult, if not impossible, to obtain. Hence, in

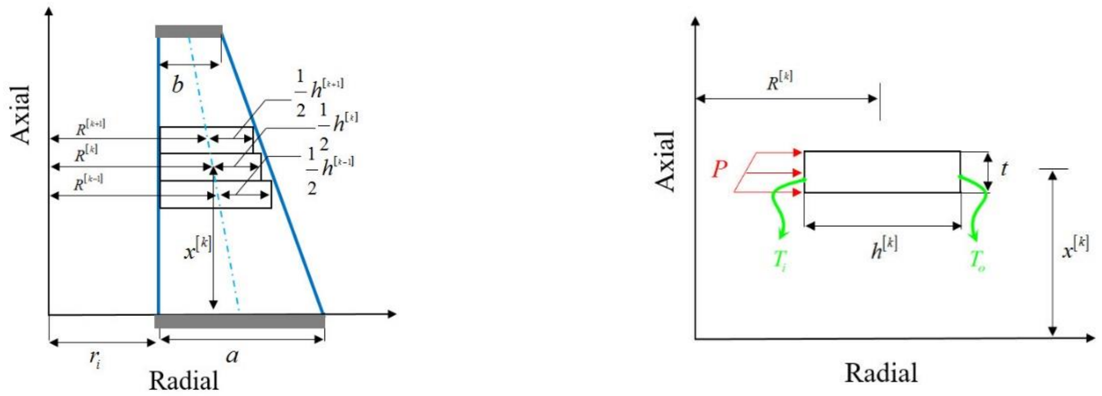

(a) (b)

Fig. 2 (a) Division of thick cylinder with variable thickness into homogenous disks with constant thickness; (b) Geometry of an arbitrary homogenous disk layer

this study, using a semi-analytical method Eq. (12) is converted to a set of non-homogenous linear differential equations with constant coefficients by dividing the cylinder into homogenous disk layers with constant thickness t, (Fig. 2(a)).Therefore, the governing equations convert to non-homogeneous set of differential equations with constant coefficients. $x^{[k]}$ and $R^{[k]}$ are length and radius of middle of disks. The length of middle of an arbitrary disk (Fig. 2(b)) is as follows

$$\begin{cases} x^{[k]} = \left(k - \dfrac{1}{2}\right)\dfrac{L}{n_L} \\ \left(x^{[k]} - \dfrac{t}{2}\right) \leq x \leq \left(x^{[k]} + \dfrac{t}{2}\right) \\ t = \dfrac{L}{n_L} \end{cases} \tag{13}$$

In Fig. 2, n_L represents the number of disks and k is the corresponding number given to each disk. The radius of middle point of each disk is as follows

$$R^{[k]} = r_i + \frac{h^{[k]}}{2}, \quad h^{[k]} = a - tan(\beta)\, x^{[k]} \tag{14}$$

Thus

$$\frac{dh^{[k]}}{dx} = 2\frac{dR^{[k]}}{dx} = -tan(\beta) \tag{15}$$

Considering shear stress and based on first-order shear deformation theory, non-homogeneous set of ordinary differential equations with constant coefficient of each disk is obtained

$$\begin{cases} [B_1]^{[k]}\dfrac{d^2}{dx^2}\{y\}^{[k]} + [B_2]^{[k]}\dfrac{d}{dx}\{y\}^{[k]} + [B_3]^{[k]}\{y\}^{[k]} = \{F\}^{[k]} \\ \{y\}^{[k]} = \left\{\dfrac{du(x)^{[k]}}{dx} \quad \phi(x)^{[k]} \quad w(x)^{[k]} \quad \psi(x)^{[k]}\right\}^T \end{cases} \tag{16}$$

2.2 Heat conduction formulation

The steady-state heat conduction equation in hollow cylinder in polar coordinates is as follow

$$\frac{d}{dr}\left[k_T r \frac{dT}{dr}\right] = 0 \tag{17}$$

where k_T is thermal conductivity of the cylinder. By considering $r = R + z$, Eq. (17) can be written as follows

$$\frac{d}{dz}\left[{k_T}^{[k]}\left(R^{[k]} + z\right)\frac{dT^{[k]}}{dz}\right] = 0 \tag{18}$$

Solving the differential Eq. (18) finally the temperature distribution is derived in the form

$$T^{[k]} = {g_1}^{[k]}\int \frac{dz}{{k_T}^{[k]}\left(R^{[k]} + z\right)} + {g_2}^{[k]} - T_{ref} \tag{19}$$

where ${g_1}^{[k]}$ and ${g_2}^{[k]}$ are the constants of integration which obtained from boundary conditions. T_{ref} represents the reference temperature where in this study assumed that $T_{ref} = T_o$.

According to Fig. 1, the inner and outer surfaces of the variable cylinder are subjected to temperatures T_i and T_o, respectively. Applying the thermal boundary conditions, the temperature distribution is obtained as

$$T^{[k]} = (T_o - T_i)\left(\left[\frac{ln\left(\dfrac{R^{[k]}+z}{R^{[k]}-\frac{h^{[k]}}{2}}\right)}{ln\left(\dfrac{R^{[k]}+\frac{h^{[k]}}{2}}{R^{[k]}-\frac{h^{[k]}}{2}}\right)}\right] - 1\right) \tag{20}$$

For thermo-elastic analysis of thick cylindrical pressure vessels the creep strains (ε_x^c,ε_θ^c,ε_z^c) are ignored. The total solution for Eq. (16) is

$$\{y\}^{[k]} = \sum_{i=1}^{6} {C_i}^{[k]}\{V\}_i^{[k]} e^{{m_i}^{[k]}x} + \left[{B_3}^{[k]}\right]^{-1}\{F\}^{[k]} \tag{21}$$

where C_i are unknown values and determine from boundary and continuity conditions, m_i and $\{V\}_i$ are eigenvalues and eigenvectors respectively.

Given that the two ends of the cylinder are clamp-clamp, then

$$\begin{Bmatrix} U_x(x,z) \\ U_z(x,z) \end{Bmatrix}_{x=0,L} = \begin{Bmatrix} 0 \\ 0 \end{Bmatrix} \tag{22}$$

According to the semi analytical solution that is used in this study, the continuity conditions based on stresses and displacements between the layers must be satisfied. The continuity conditions are as follows

$$\begin{cases} \begin{Bmatrix} U_x{}^{[k-1]}(x,z) \\ U_z{}^{[k-1]}(x,z) \end{Bmatrix}_{x=x^{[k-1]}+\frac{t}{2}} = \begin{Bmatrix} U_x{}^{[k]}(x,z) \\ U_z{}^{[k]}(x,z) \end{Bmatrix}_{x=x^{[k]}-\frac{t}{2}} \\ \begin{Bmatrix} \dfrac{dU_x{}^{[k-1]}(x,z)}{dx} \\ \dfrac{dU_z{}^{[k-1]}(x,z)}{dx} \end{Bmatrix}_{x=x^{[k-1]}+\frac{t}{2}} = \begin{Bmatrix} \dfrac{dU_x{}^{[k]}(x,z)}{dx} \\ \dfrac{dU_z{}^{[k]}(x,z)}{dx} \end{Bmatrix}_{x=x^{[k]}-\frac{t}{2}} \\ \begin{Bmatrix} U_x{}^{[k]}(x,z) \\ U_z{}^{[k]}(x,z) \end{Bmatrix}_{x=x^{[k]}+\frac{t}{2}} = \begin{Bmatrix} U_x{}^{[k+1]}(x,z) \\ U_z{}^{[k+1]}(x,z) \end{Bmatrix}_{x=x^{[k+1]}-\frac{t}{2}} \\ \begin{Bmatrix} \dfrac{dU_x{}^{[k]}(x,z)}{dx} \\ \dfrac{dU_z{}^{[k]}(x,z)}{dx} \end{Bmatrix}_{x=x^{[k]}+\frac{t}{2}} = \begin{Bmatrix} \dfrac{dU_x{}^{[k+1]}(x,z)}{dx} \\ \dfrac{dU_z{}^{[k+1]}(x,z)}{dx} \end{Bmatrix}_{x=x^{[k+1]}-\frac{t}{2}} \end{cases} \tag{23}$$

For isotropic cylinder with creep behavior, the relations between rates of stress and strain are

$$\begin{cases} \begin{Bmatrix} \dot{\sigma}_x \\ \dot{\sigma}_\theta \\ \dot{\sigma}_z \end{Bmatrix} = \lambda E \begin{bmatrix} 1-\upsilon & \upsilon & \upsilon \\ \upsilon & 1-\upsilon & \upsilon \\ \upsilon & \upsilon & 1-\upsilon \end{bmatrix} \begin{Bmatrix} \dot{\varepsilon}_x - \dot{\varepsilon}_x^c \\ \dot{\varepsilon}_\theta - \dot{\varepsilon}_\theta^c \\ \dot{\varepsilon}_z - \dot{\varepsilon}_z^c \end{Bmatrix} \\ \dot{\tau}_{xz} = \lambda E \left(\dfrac{1-2\upsilon}{2} \right) \dot{\gamma}_{xz} \end{cases} \tag{24}$$

where $\dot{\sigma}_i$, $\dot{\varepsilon}_i$ and $\dot{\varepsilon}_i^c$ are, respectively, stress rates, strain rates and the creep strain rates in the axial, circumferential and radial directions, also $\dot{\tau}_{xz}$ and $\dot{\gamma}_{xz}$ are the shear stress rate and shear strain rate, respectively. Using Norton's law calculate as follows

$$\begin{cases} \begin{Bmatrix} \dot{\varepsilon}_x^c \\ \dot{\varepsilon}_\theta^c \\ \dot{\varepsilon}_z^c \end{Bmatrix} = \dfrac{A\sigma_e{}^{(n-1)}}{2} \begin{bmatrix} 2 & -1 & -1 \\ -1 & 2 & -1 \\ -1 & -1 & 2 \end{bmatrix} \begin{Bmatrix} \sigma_x \\ \sigma_\theta \\ \sigma_z \end{Bmatrix} \\ \sigma_e = \dfrac{1}{\sqrt{2}} \sqrt{(\sigma_x-\sigma_\theta)^2 + (\sigma_x-\sigma_z)^2 + (\sigma_z-\sigma_\theta)^2 + 6\tau_{xz}{}^2} \end{cases} \tag{25}$$

where A and n are material constants for creep. Using Eq. (9) and considering the pressure to be constant with time, the equilibrium equation for creep analysis is

$$\begin{cases} \dfrac{d}{dx}\left(R\dot{N}_x\right) = 0 \\ \dfrac{d}{dx}\left(R\dot{Q}_x\right) - \dot{N}_\theta = 0 \\ \dfrac{d}{dx}\left(R\dot{M}_x\right) - R\dot{Q}_x = 0 \\ \dfrac{d}{dx}\left(R\dot{M}_{xz}\right) - \dot{M}_\theta - R\dot{N}_z = 0 \end{cases} \tag{26}$$

Considering the temperature field to be steady, the following set of differential equations for displacement rates is obtained

$$\begin{cases} [B_1]\dfrac{d^2}{dx^2}\{\dot{y}\} + [B_2]\dfrac{d}{dx}\{\dot{y}\} + [B_3]\{\dot{y}\} = \{F_c\} \\ \{\dot{y}\} = \begin{Bmatrix} \dfrac{d\dot{u}(x)}{dx} & \dot{\phi}(x) & \dot{w}(x) & \dot{\psi}(x) \end{Bmatrix}^T \end{cases} \tag{27}$$

where the force vector $\{F_c\}_{4\times1}$ has been defined in the Appendix B. The total solution for Eq. (27) is

$$\{\dot{y}\}^{[k]} = \sum_{i=1}^{6} D_i{}^{[k]} \{V\}_i{}^{[k]} e^{m_i{}^{[k]}x} + \left[B_3{}^{[k]}\right]^{-1} \{F_c\}^{[k]} \tag{28}$$

where D_i are unknown values. When the stress rate is known, the calculation of stresses at any time t_i should be performed iteratively

$$\begin{cases} \sigma_r^{(i)}(t_i) = \sigma_r^{(i-1)}(t_{i-1}) + \dot{\sigma}_r^{(i)}(t_i)dt^{(i)} \\ \sigma_\theta^{(i)}(t_i) = \sigma_\theta^{(i-1)}(t_{i-1}) + \dot{\sigma}_\theta^{(i)}(t_i)dt^{(i)} \\ \sigma_x^{(i)}(t_i) = \sigma_x^{(i-1)}(t_{i-1}) + \dot{\sigma}_x^{(i)}(t_i)dt^{(i)} \\ \tau_{rx}^{(i)}(t_i) = \tau_{rx}^{(i-1)}(t_{i-1}) + \dot{\tau}_{rx}^{(i)}(t_i)dt^{(i)} \end{cases} \tag{29}$$

where

$$t_i = \sum_{k=0}^{i} dt^{(k)} \tag{30}$$

The solution of $t_i = 0$ corresponds to that for thermo-elastic material behavior. To calculate $\dot{\sigma}_{ij}^{(i)}(r,t_i)$, the stresses at the time t_{i-1} used.

3. Creep damage and remaining life assessment

The most used method for creep damage calculating is Robinson's linear life-fraction rule. According to this method, the fracture under variable load and temperatures can be predicted adding the creep life fractions consumed at each condition until their sum reaches the value of unity. The calculation of accumulated creep damage is performed at the end of each time increment Δt^i by using the following equation

$$D_f^i = \sum_{i=1}^{n} \frac{\Delta t^i}{t_r^i} \tag{31}$$

where D_f^i is creep damage and t_r^i is the creep fracture time at *i-th* time increment and at the equivalent stress and temperature of that point in the radial direction of the cylinder. At rupture, $D_f^i = 1$, which is the rupture criteria.

The time to rupture is calculated using LMP. In contrast to the conventional creep tests, which take a long time, the LMP can be obtained using some sort of quick tests at high temperature and stress level and then extrapolating the

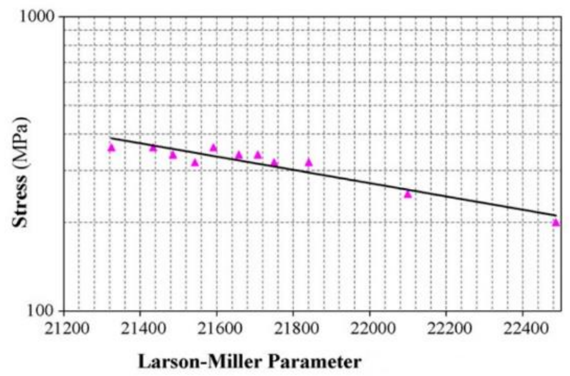

Fig .3 Variation of stress versus Larson–Miller parameter for the 304L SS (Tahami *et al*. 2010)

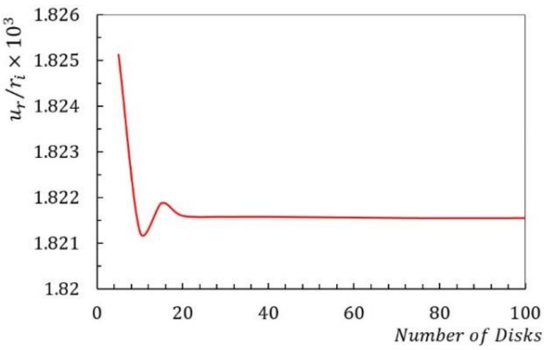

Fig. 4 Variation of normalized radial displacement along the number of disk layers ($m_p = 1$)

results for prediction of the required parameters. The Larson–Miller parameter is a grouping concept between rupture time (t_r) and temperature (T) for a particular stress level (Tahami *et al*. 2010). The Larson-Miller extrapolation parameter is in the following form

$$P_{LM}^i = T.(C + log_{10}(t_r^i)) \tag{32}$$

In this equation T is in Kelvin, t_r^i is in hours and C is a physical parameter which has been assumed to be 20. This value is an accepted amount for most engineering materials and steels (Larson 1952) and therefore, has been used in this study to estimate the creep behaviour of the material. The LMP can be easily used to creep fracture data extrapolation, in which for any constant stress level the combination of rupture time and test temperature, the LMP will remain constant (Tahami *et al*. 2010): LMP variation with stress is shown in Fig. 3. The remaining life at any point in the radial direction of the cylinder is then given by

$$RL^i = \left(1 - D_f^i\right)t_r^i \tag{33}$$

4. Numerical results and discussion

In this section, numerical results are presented and discussed for verifying the accuracy of the present theory in predicting creep stress responses of cylinder. The geometrical characteristics of pressure vessel are assumed as $r_i = 400\,mm$, $a = 40\,mm$, $b = 20\,mm$ and $L = 2000\,mm$. 304L Austenitic stainless steel (304L ASS) is being used in this paper as material due to its excellent creep resistance. Type 304L is an extra low-carbon variation of type 304 with a 0.03% maximum carbon content that eliminates carbide precipitation due to welding. The following data for loading and material properties for type 304L are used in this investigation (Tahami *et al*. 2010)

$$E = 179\,GPa, \quad \upsilon = 0.3, \quad \alpha = 16.9 \times 10^{-6}\,{}^{o}C,$$
$$k_T = 16.2\,\frac{W}{m\,{}^{o}C}, \quad P_1 = 20\,MPa, \quad P_2 = 10\,MPa$$
$$A = 7.18 \times 10^{-43}\,Pa^{-n}s^{-1}, \quad n = 5.7278$$

The boundary conditions for temperature are taken as $T_i = 600\,{}^{o}C$ and $T_o = 550\,{}^{o}C$. The results are presented in a non-dimensional form. Displacements are normalized

Table 1 Numerical results based on first-order shear deformation theory (FSDT) and FEM at different creep times layer ($m_p = 1$)

		Initial solution	t = 500 hr	t = 1000 hr	t = 2000 hr
$\frac{u_r}{r_i} \times 10^3$	FSDT	1.6501	1.7301	1.8215	1.9501
	FEM	1.6521	1.7511	1.8365	1.9845
$\frac{u_x}{r_i} \times 10^3$	FSDT	0.0225	0.0139	0.0102	0.0085
	FEM	0.0807	0.0689	0.0562	0.0304
$\frac{\sigma_r}{\bar{P}}$	FSDT	-0.6988	-0.6572	-0.6142	-0.6174
	FEM	-0.6038	-0.5824	-0.5690	-0.5514
$\frac{\sigma_\theta}{\bar{P}}$	FSDT	13.3211	13.5468	13.7689	13.7348
	FEM	13.4173	13.5960	13.6633	13.6906
$\frac{\sigma_x}{\bar{P}}$	FSDT	-1.6626	-1.1766	-0.7175	0.0183
	FEM	1.5192	-0.9135	-0.4103	0.3940
$\frac{\tau_{rx}}{\bar{P}}$	FSDT	-0.0095	-0.0120	-0.0139	-0.0167
	FEM	-0.0108	-0.0134	-0.0153	-0.0180
$\frac{\sigma_e}{\bar{P}}$	FSDT	14.5260	14.4707	14.4351	14.0452
	FEM	14.5006	14.3466	14.1540	13.7940

by dividing to the internal radius. In order to normalize stresses, we define the mean internal pressure parameter as follows

$$\bar{P} = \frac{(P_1 + P_2)}{2} \tag{34}$$

The number of disk layers have significant effect on the results. In order to show the effectiveness of disk layers, variation of normalized radial displacement along the number of disks is shown in Fig. 4. It could be observed that if the number of disk layers is more than 40, there will be no significant effect on radial displacement and other results. In the present study, 75 disks are used.

In order to show the effectiveness and accuracy of the approach suggested here, a comparison between responses of the present theory and FEM can be made. In FEM, a thick cylinder was modeled using ANSYS®. The PLANE 223 element in axisymmetric mode, which is an element with eight nodes with up to four degrees of freedom per each node, was used for discretization. There is a very good agreement among numerical results based on first-order shear deformation theory and FEM at different creep times. Table 1 presents the results of the different solutions for the thick cylinder under mechanical and thermal loading at the middle layer and $x = \frac{L}{2}$, after 0 hr (initial solution), 500 hr, 1000 hr and 2000 hr of creeping.

Fig. 5 illustrates the finite-element model is established with ANSYS® after 1000 hr of creeping.

Relevant results have also been obtained for the displacements and creep stresses curves at different layers through the axial direction of the shell in Figs. 6 and 7, which verify the results obtained in Table 1.

Figs. 6 and 7 show that the semi-analytical solution based on first-order shear deformation theory has an acceptable accuracy. Also, it observed that first-order shear deformation theory method is very suitable for the purpose of calculation of radial stress, circumferential stress, shear stress and radial displacement. However, first-order shear deformation theory is not that useful for axial stress and not useful at all for axial displacement.

It could be observed from Fig. 6(a) that there is no significant changes in the variation of normalized radial displacement at different layers. According to Fig. 6(b), the greatest axial displacement occurs in the internal surface.

According to Fig. 7, the different behavior of the stress distribution near the clamped boundaries is due to the edge moments in these regions. As shown in Figs. 7(a) and (d), at the points near the boundaries, the absolute maximum of radial and shear creep stresses occur at the outer surface of the cylinder. Fig. 7(b) show that the absolute maximum of circumferential creep stress occur at the outer surface of the cylinder. It can be seen from Fig. 7(c) that at the points

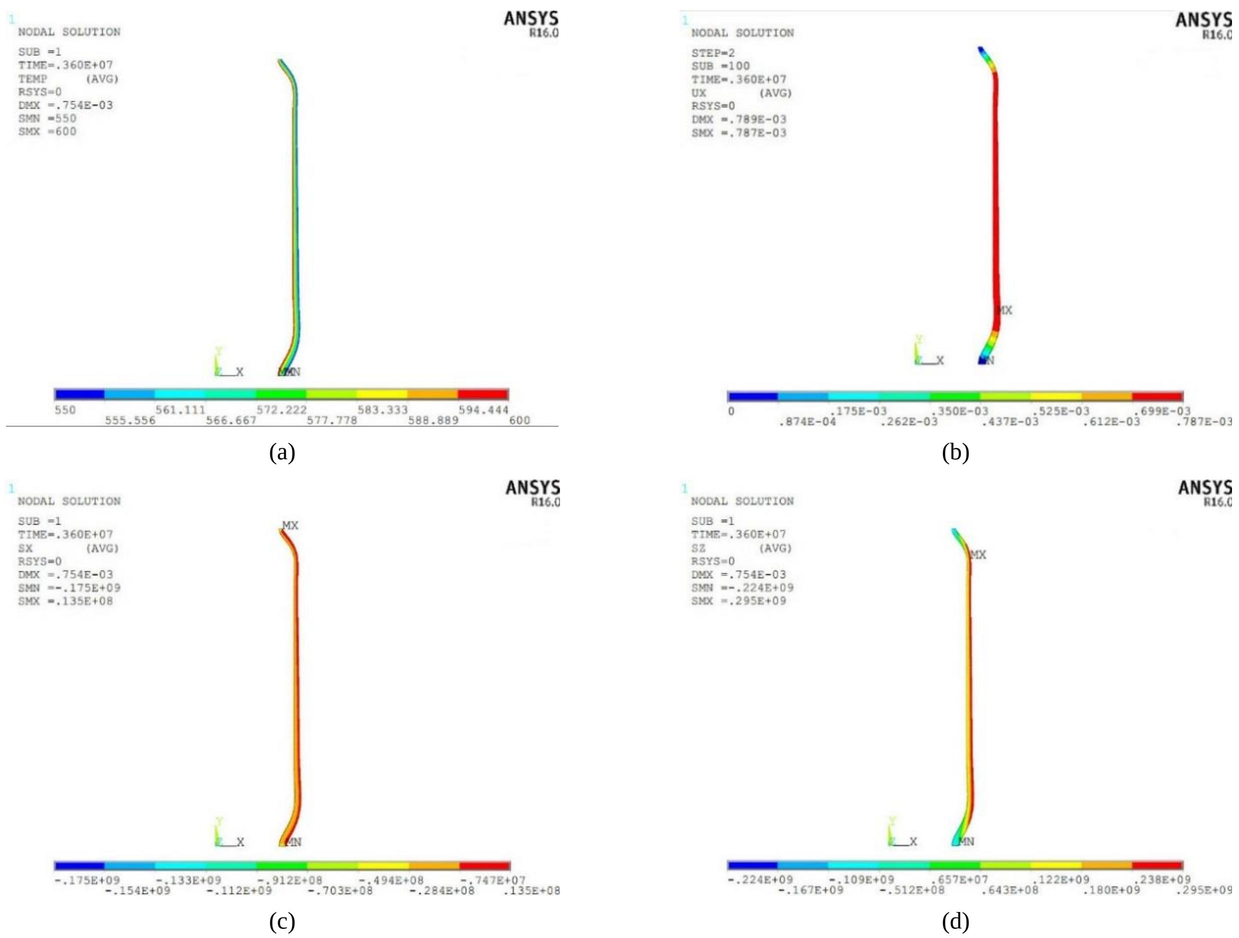

Fig. 5 Finite-element model for the cylinder (a) Temperature gradient; (b) Radial displacement; (c) Radial stress; (d) Circumferential stress distribution in the cylinder after 1000 hr of creeping

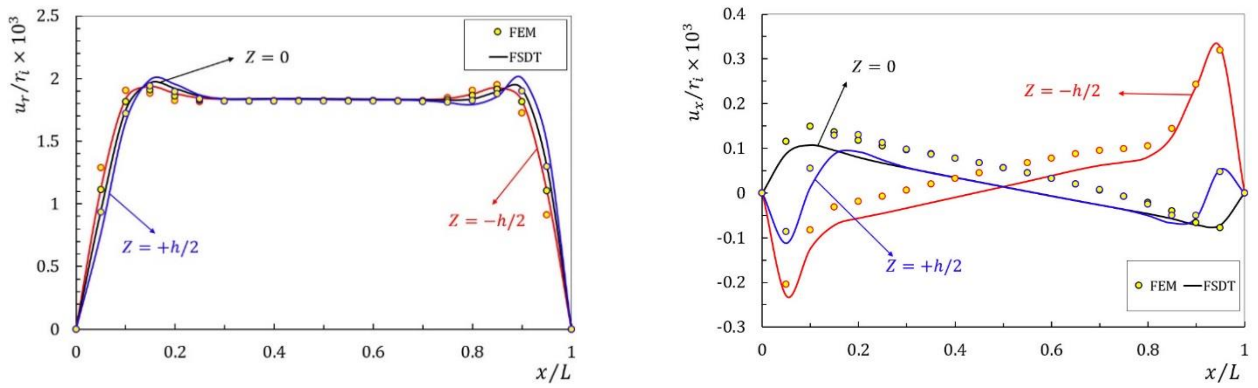

(a) (b)

Fig. 6 Variation of normalized radial and axial displacement along the dimensionless axial direction after 1000 hr of creeping at different layers ($m_p = 1$)

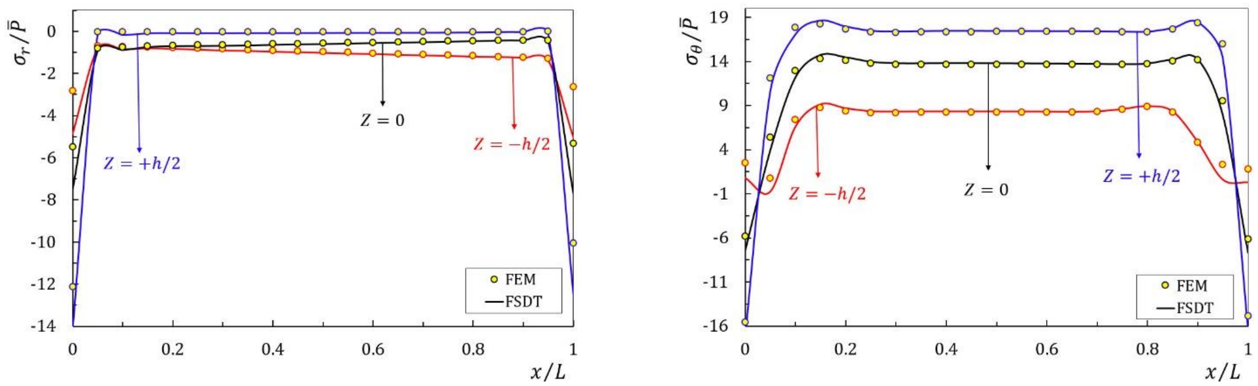

(a) (b)

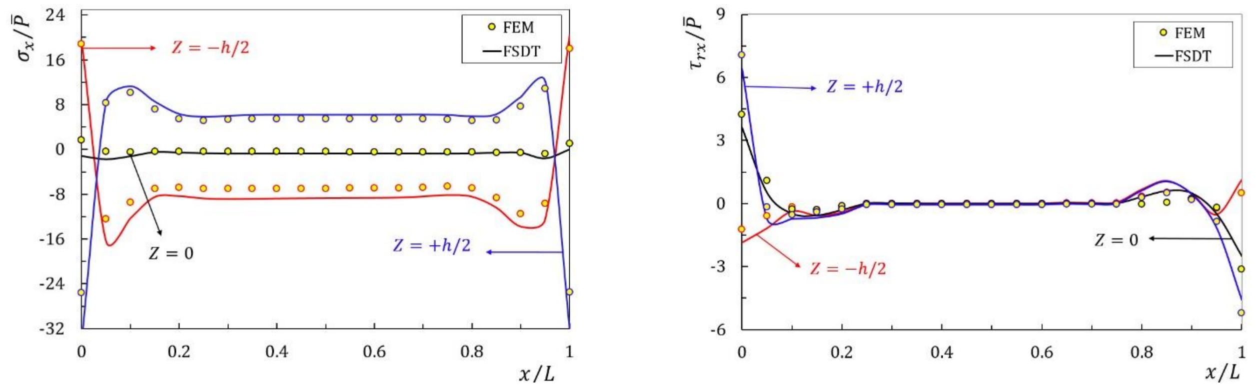

(c) (d)

Fig. 7 Variation of normalized creep stresses along the dimensionless axial direction after 1000 hr of creeping at different layers ($m_p = 1$)

away from boundaries, the axial stress changes from negative values to positive along the thickness of the cylinder.

The distribution of pressure for different values of m_p could be seen in Fig. 8 after 1000 hr of creeping. Fig. 8(a) shows that a linear pressure distribution can be obtained by setting $m_p = 1$. It can be seen from Figs. 8(b) and (d) that, with increasing non-uniformity pressure constant m_p, radial displacement and effective stress increase. It can be observed from Fig. 8(c) that the maximums of axial displacement occur for $m_p = 0$.

Effective stress distribution of the cylindrical vessel under an applied non-uniform internal pressure and temperature field up to 70000 hr of creeping, along the dimensionless radial at $x = \frac{L}{2}$, is shown in Fig. 9(a). It can be seen from Fig. 9(a) that the effective stresses are decreasing with time during the life of the vessel. Fig. 9(b) shows the effect of internal pressure on normalized effective stress. It is clear that with increasing internal pressure, effective stress increases.

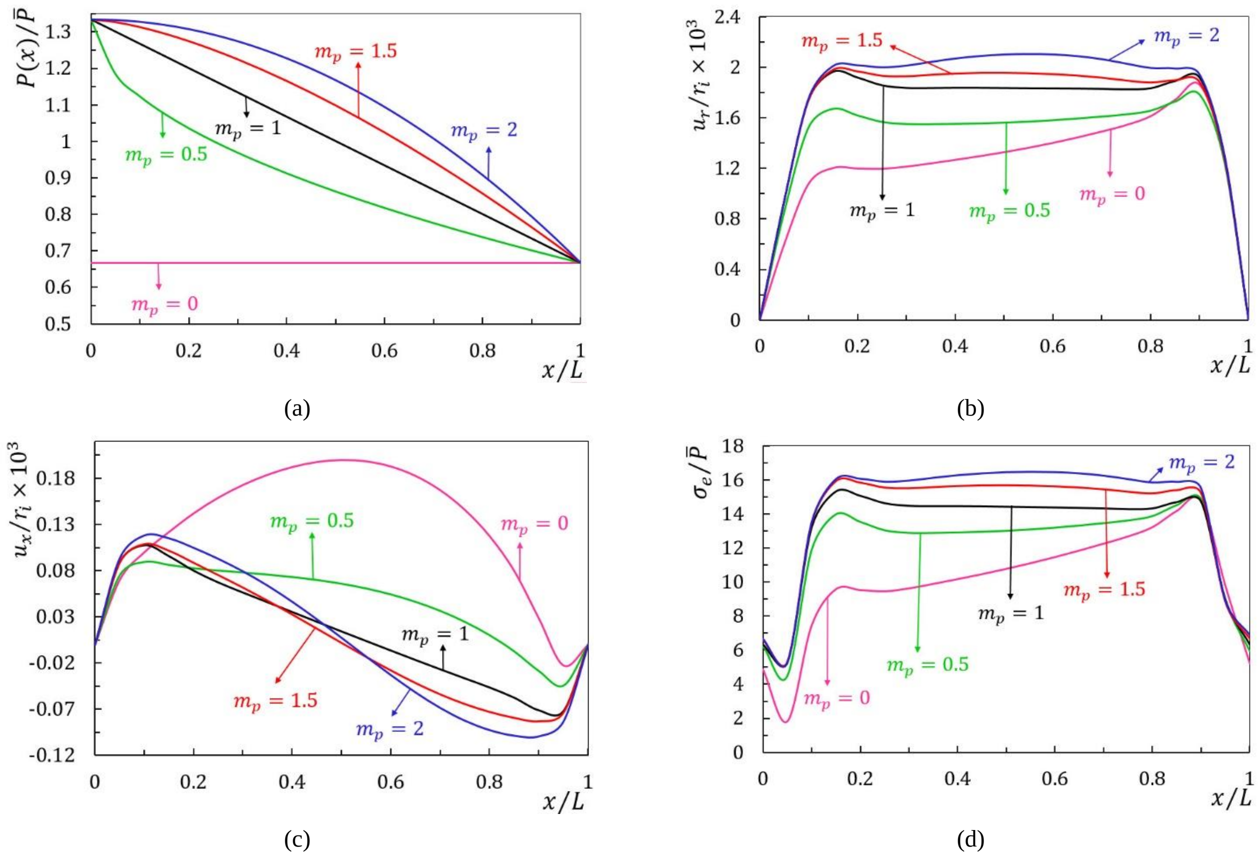

Fig. 8 Effect of the non-uniformity pressure constant on the normalized (a) pressure profile; (b) radial displacement; (c) axial displacement; (d) effective stress along the dimensionless axial direction after 1000 hr of creeping in middle layer

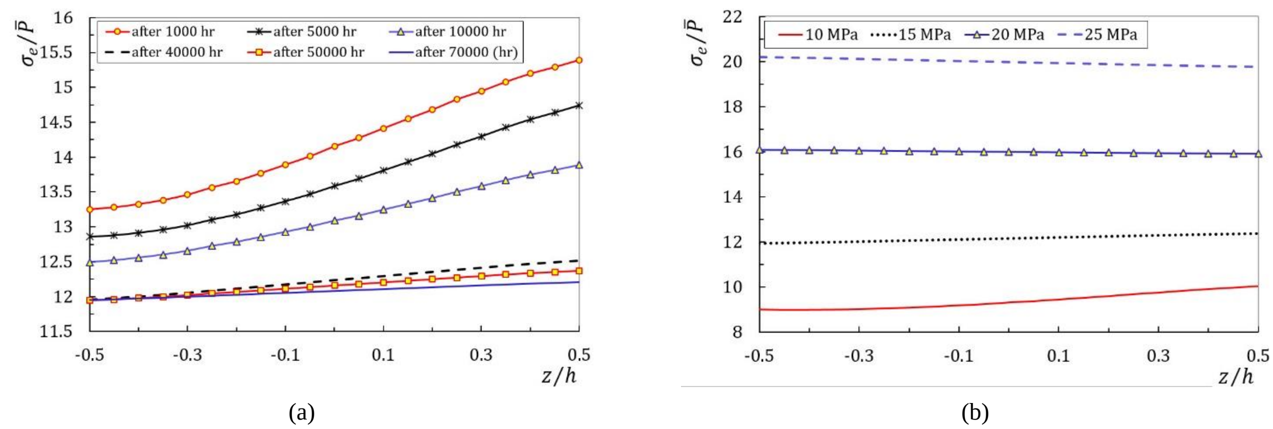

Fig. 9 (a) Variation of normalized effective stress along the dimensionless radial direction ($m_p = 1$); (b) Effect of internal pressure on normalized effective stress

Creep damage and effect of internal pressure on creep damage histories are illustrated in Figs. 10(a) and (b). Figs. 11(a) and (b) also show the remaining life and effect of internal pressure on remaining life histories along the dimensionless radial direction of the cylinder at $x = \frac{L}{2}$. Maximum damages and the minimum remaining lives are located at the inner surface of the cylinder as illustrated in Figs. 10 and 11. It can be seen from Figs. 10(b) and 11(b) that with increasing internal pressure, creep damages increase and remaining lives decrease.

Effect of temperature gradient on creep damage and remaining life histories are illustrated in Figs. 12(a) and (b). It can be seen that, increasing temperature gradient has increased creep damages and decreased remaining lives.

Creep damage and life assessment of isotropic thick-walled cylindrical pressure vessels with variable thickness subjected to the temperature gradient and internal non-uniform pressure made of 304L austenitic stainless steel has been investigated in the present study by taking into

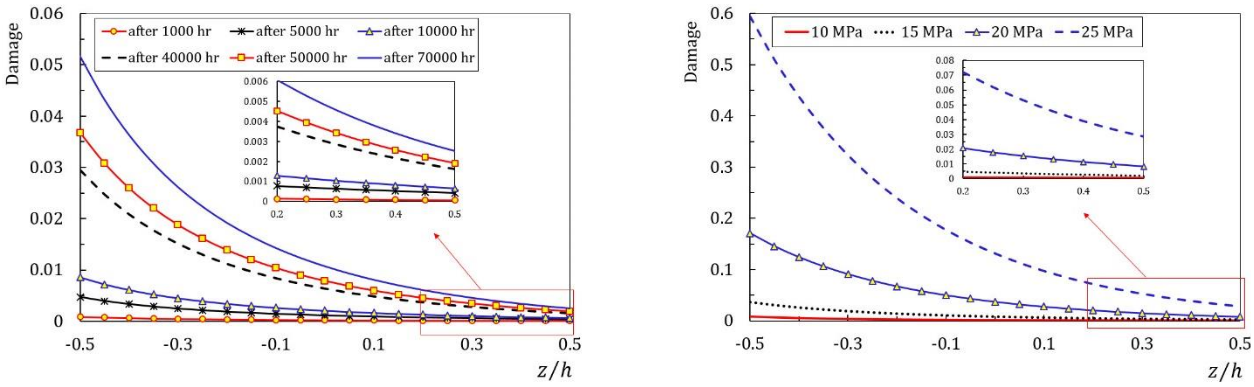

(a) (b)

Fig. 10 (a) Variation of creep damage along the dimensionless radial direction ($m_p = 1$); (b) Effect of internal pressure on creep damage distribution ($m_p = 1$)

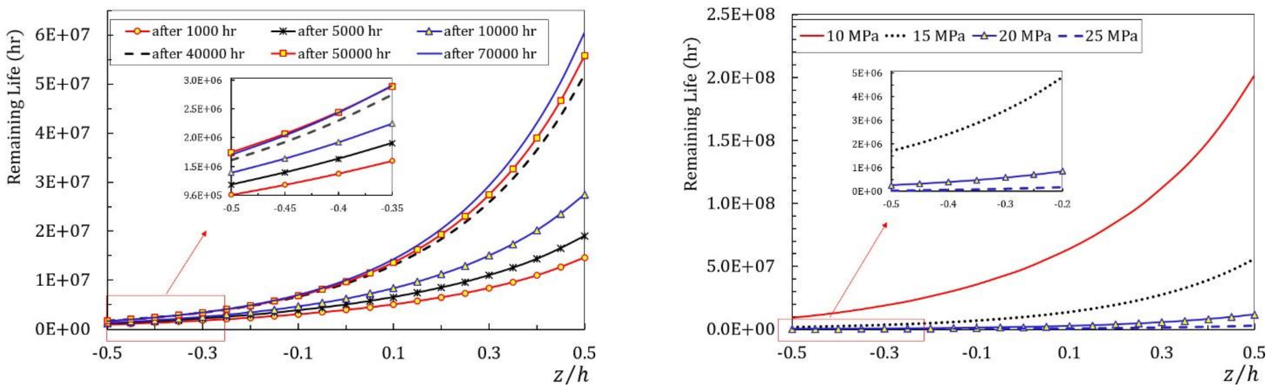

(a) (b)

Fig. 11 (a) Variation of remaining life along the dimensionless radial direction ($m_p = 1$); (b) Effect of internal pressure on remaining life distribution ($m_p = 1$)

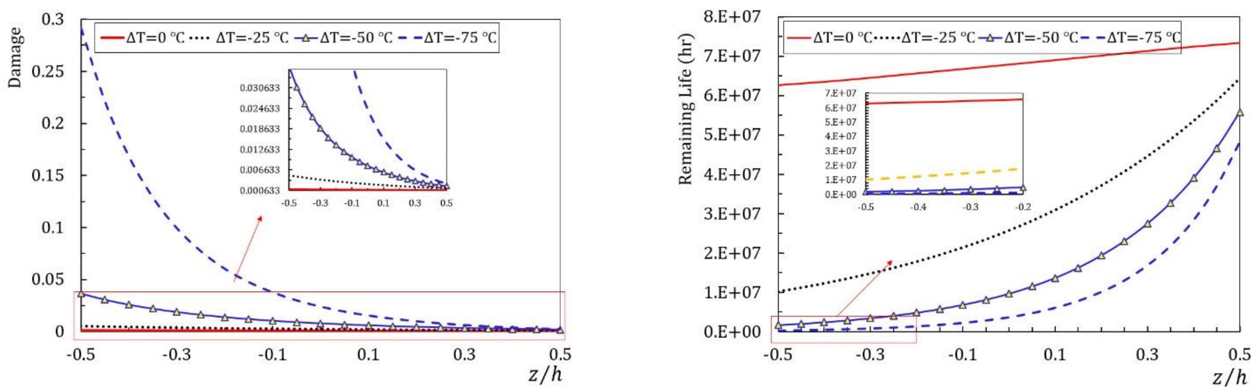

(a) (b)

Fig. 12 Effect of temperature gradient on (a) creep damage; (b) remaining life distributions ($m_p = 1$)

account the creep behavior, as described by Norton's model. The governing equations are based on first-order shear deformation theory that accounts for the transverse shear. Using the semi-analytical solution, the thick cylindrical shell with variable thickness is divided into disks with constant height. Considering continuity between layers and applying boundary conditions, the governing set of differential equations with constant coefficients are solved. The creep damage obtained by Robinson's linear life fraction damage rule and LMP is used to obtain creep remaining life assessment. The results obtained for stresses and displacements are compared with the solutions carried out through the FEM. Good agreement is found among the results.

The following conclusions are made in this investigation:

- The results obtained using the first-order shear deformation theory in comparison with the FEM results are in good adaptation specially for obtaining creep radial, circumferential and shear stresses and radial displacement.
- Due to the edge moments near the clamped boundaries, the stress distributions in these regions have different behavior in comparison with the other parts of the cylinder.
- The radial creep displacement values for cylinder are greater than the axial creep displacement.
- Effective stresses are decreasing with time throughout the thickness during the life of the vessel.
- The maximum creep life is located at the outer surface of the cylinder where the minimum value of temperature is located.
- Increasing internal pressure and temperature gradient have considerably increased creep damages and decreased the remaining life of the vessel.
- The shells with different geometries, loadings and boundary conditions could be analyzed and solved using the semi-analytical solution presented in this study.

References

Abdelaziz, H.H., Meziane, M.A.A., Bousahla, A.A., Tounsi, A., Mahmoud, S.R. and Alwabli, A.S. (2017), "An efficient hyperbolic shear deformation theory for bending, buckling and free vibration of FGM sandwich plates with various boundary conditions", *Steel Compos. Struct., Int. J.*, **25**(6), 693-704. https://doi.org/10.12989/scs.2017.25.6.693

Afshin, A., Nejad, M.Z. and Dastani, K. (2017), "Transient thermoelastic analysis of FGM rotating thick cylindrical pressure vessels under arbitrary boundary and initial conditions", *J. Comput. Appl. Mech.*, **48**(1), 15-26. https://doi.org/10.22059/JCAMECH.2017.233643.144

Altenbach, H., Gorash, Y. and Naumenko, K. (2008), "Steady-state creep of a pressurized thick cylinder in both the linear and the power law ranges", *Acta Mech.*, **195**, 263-274. https://doi.org/10.1007/s00707-007-0546-5

Carroll, B.E., Otis, R.A., Borgonia, J.P., Suh, J.-o., Dillon, R.P., Shapiro, A.A., Hofmann, D.C., Liu, Z.-K. and Beese, A.M. (2016), "Functionally graded material of 304L stainless steel and inconel 625 fabricated by directed energy deposition: Characterization and thermodynamic modeling", *Acta Mater.*, **108**, 46-54. https://doi.org/10.1016/j.actamat.2016.02.019

Dehghan, M., Nejad, M.Z. and Moosaie, A. (2016), "Thermo-electro-elastic analysis of functionally graded piezoelectric shells of revolution: Governing equations and solutions for some simple cases", *Int. J. Eng. Sci.*, **104**, 34-61. https://doi.org/10.1016/j.ijengsci.2016.04.007

Dung, D.V. and Dong, D.T. (2016), "Post-buckling analysis of functionally graded doubly curved shallow shells reinforced by FGM stiffeners with temperature-dependent material and stiffener properties based on TSDT", *Mech. Res. Commun.*, **78**, 28-41. https://doi.org/10.1016/j.mechrescom.2016.09.008

Fatehi, P. and Nejad, M.Z. (2014), "Effects of material gradients on onset of yield in FGM rotating thick cylindrical shells", *Int. J. Appl. Mech.*, **6**(4), Article Number: 1450038. https://doi.org/10.1142/S1758825114500380

Ghannad, M. and Nejad, M.Z. (2010), "Elastic analysis of pressurized thick hollow cylindrical shells with clamped-clamped ends", *Mechanika*, **85**(5), 11-18. https://doi.org/10.5755/j01.mech.85.5.15963

Ghannad, M. Nejad, M.Z. and Rahimi, G.H. (2009), "Elastic solution of axisymmetric thick truncated conical shells based on first-order shear deformation theory", *Mechanika*, **79**(5), 13-20. https://doi.org/10.5755/j01.mech.79.5.15476

Ghannad, M., Nejad, M.Z., Rahimi, G.H. and Sabouri, H. (2012), "Elastic analysis of pressurized thick truncated conical shells made of functionally graded materials", *Struct. Eng. Mech., Int. J.*, **43**(1), 105-126. https://doi.org/10.12989/sem.2012.43.1.105

Ghannad, M., Rahimi, G.H. and Nejad, M.Z. (2013), "Elastic analysis of pressurized thick cylindrical shells with variable thickness made of functionally graded materials", *Compos. Part B-Eng.*, **45**(1), 388-396. https://doi.org/10.1016/j.compositesb.2012.09.043

Gharibi, M., Nejad, M.Z. and Hadi, A. (2017), "Elastic analysis of functionally graded rotating thick cylindrical pressure vessels with exponentially-varying properties using power series method of Frobenius", *J. Comput. Appl. Mech.*, **48**(1), 89-98. https://doi.org/10.22059/jcamech.2017.233633.143

Hadi, A., Nejad, M.Z.. Rastgoo, A. and Hosseini, M. (2018a), "Buckling analysis of FGM Euler-Bernoulli nano-beams with 3D-varying properties based on consistent couple-stress theory", *Steel Compos. Struct., Int. J.*, **26**(6), 663-672. https://doi.org/10.12989/scs.2018.26.6.663

Hadi, A., Nejad, M.Z. and Hosseini, M. (2018b), "Vibrations of three-dimensionally graded nanobeams", *Int. J. Eng. Sci.*, **128**, 12-23. https://doi.org/10.1016/j.ijengsci.2018.03.004

Jabbari, M., Nejad, M.Z. and Ghannad, M. (2015), "Thermo-elastic analysis of axially functionally graded rotating thick cylindrical pressure vessels with variable thickness under mechanical loading", *Int. J. Eng. Sci.*, **96**, 1-18. https://doi.org/10.1016/j.ijengsci.2015.07.005

Jabbari, M., Nejad, M.Z. and Ghannad, M. (2016), "Thermo-elastic analysis of axially functionally graded rotating thick truncated conical shells with varying thickness", *Compos. Part B-Eng.*, **96**, 20-34. https://doi.org/10.1016/j.compositesb.2016.04.026

Jandaghian, A.A. and Rahmani, O. (2017), "Vibration analysis of FG nanobeams based on third-order shear deformation theory under various boundary conditions", *Steel Compos. Struct., Int. J.*, **25**(1), 67-78. https://doi.org/10.12989/scs.2017.25.1.067

Jemielita, G. (2002), "Coefficients of shear correction in transversely nonhomogeneous moderately thick plates", *J. Theor. Appl. Mech.*, **40**, 73-84.

Kassner, M., Smith, K. and Campbell, C. (2015), "Low-temperature creep in pure metals and alloys", *J. Mater. Sci.*, **50**, 6539-6551. https://doi.org/10.1007/s10853-015-9219-2

Kashkoli, M.D. and Nejad, M.Z. (2014), "Effect of heat flux on creep stresses of thick-walled cylindrical pressure vessels", *J. Appl. Res. Technol.*, **12**(3), 585-597.

Kashkoli, M.D. and Nejad, M.Z. (2015), "Time-dependent thermo-elastic creep analysis of thick-walled spherical pressure vessels made of functionally graded materials", *J. Theor. Appl. Mech.*, **53**(4), 1053-1065. https://doi.org/10.15632/jtam-pl.53.4.1053

Kashkoli, M.D. and Nejad, M.Z. (2018), "Time-dependent creep analysis and life assessment of 304 L austenitic stainless steel thick pressurized truncated conical shells", *Steel Compos. Struct., Int. J.*, **28**(3), 349-362. https://doi.org/10.12989/scs.2018.28.3.349

Kashkoli, M.D., Tahan, K.N. and Nejad, M.Z. (2017a), "Time-dependent creep analysis for life assessment of cylindrical vessels using first order shear deformation theory", *J. Mech.*,

33(4), 461-474. https://doi.org/10.1017/jmech.2017.6
Kashkoli, M.D., Tahan, K.N. and Nejad, M.Z. (2017b), "Time-dependent thermomechanical creep behavior of FGM thick hollow cylindrical shells under non-uniform internal pressure", *Int. J. Appl. Mech.*, **9**(6), Article Number: 1750086. https://doi.org/10.1142/S1758825117500867
Kashkoli, M.D., Tahan, K.N. and Nejad, M.Z. (2018), "Thermomechanical creep analysis of FGM thick cylindrical pressure vessels with variable thickness", *Int. J. Appl. Mech.*, **10**(1), Article Number: 1850008. https://doi.org/10.1142/S1758825118500084
Khanna, K., Gupta, V. and Nigam, S. (2017), "Creep analysis in functionally graded rotating disc using tresca criterion and comparison with von-mises criterion", *Mater. Today*, **4**, 2431-2438. https://doi.org/10.1016/j.matpr.2017.02.094
Kobelev, V. (2014), "Some basic solutions for nonlinear creep", *Int. J. Solids Struct.*, **51**, 3372-3381. https://doi.org/10.1016/j.ijsolstr.2014.05.029
Larson, F.R. (1952), "A time temperature relationship for rupture and creep stress", *Trans. ASME*, 765-775.
Li, L. and Hu, Y. (2016), "Nonlinear bending and free vibration analyses of nonlocal strain gradient beams made of functionally graded material", *Int. J. Eng. Sci.*, **107**, 77-97. https://doi.org/10.1016/j.ijengsci.2016.07.011
Li, L., Hu, Y. and Ling, L. (2015), "Flexural wave propagation in small-scaled functionally graded beams via a nonlocal strain gradient theory", *Compos. Struct.*, **133**, 1079-1092. https://doi.org/10.1016/j.compstruct.2015.08.014
Li, L., Li, X. and Hu, Y. (2016), "Free vibration analysis of nonlocal strain gradient beams made of functionally graded material", *Int. J. Eng. Sci.*, **102**, 77-92. https://doi.org/10.1016/j.ijengsci.2016.02.010
Loghman, A. and Wahab, M.A. (1996), "Creep damage simulation of thick-walled tubes using the Θ projection concept", *Int. J. Pres. Ves. Pip.*, **67**, 105-111. https://doi.org/10.1016/0308-0161(94)00175-8
Loghman, A., Arani, A.G., Amir, S. and Vajedi, A. (2010), "Magnetothermoelastic creep analysis of functionally graded cylinders", *Int. J. Pres. Ves. Pip.*, **87**, 389-395. https://doi.org/10.1016/j.ijpvp.2010.05.001
Loghman, A., Aleayoub, S. and Sadi, M.H. (2012), "Time-dependent magnetothermoelastic creep modeling of FGM spheres using method of successive elastic solution", *Appl. Math. Model.*, **36**, 836-845. https://doi.org/10.1016/j.apm.2011.07.038
Lopez, H. and Zhang, H. (2014), "Nanoceria coating imperfections and their effect on the high-temperature oxidation resistance of a 304 stainless steel", *J. Mater. Sci.*, **49**, 277-286. https://doi.org/10.1007/s10853-013-7702-1
Mahmoud, S.R. (2017), "A new simple three-unknown shear deformation theory for bending analysis of FG plates resting on elastic foundations", *Steel Compos. Struct., Int. J.*, **25**(6), 717-726. https://doi.org/10.12989/scs.2017.25.6.717
Mazarei, Z., Nejad, M.Z. and Hadi, A. (2016), "Thermo-elasto-plastic analysis of thick-walled spherical pressure vessels made of functionally graded materials", *Int. J. Appl. Mech.*, **8**(4), Article Number: 1650054. https://doi.org/10.1142/S175882511650054X
Naumenko, K. and Altenbach, H. (2007), *Modeling of Creep for Structural Analysis*, Springer-Verlag Berlin Heidelberg, Berlin, Germany.
Nejad, M.Z. and Fatehi, P. (2015), "Exact elasto-plastic analysis of rotating thick-walled cylindrical pressure vessels made of functionally graded materials", *Int. J. Eng. Sci.*, **86**, 26-43. https://doi.org/10.1016/j.ijengsci.2014.10.002
Nejad, M.Z. and Hadi, A. (2016a), "Non-local analysis of free vibration of bi-directional functionally graded Euler-Bernoulli nano-beams", *Int. J. Eng. Sci.*, **105**, 1-11. https://doi.org/10.1016/j.ijengsci.2016.04.011
Nejad, M.Z. and Hadi, A. (2016b), "Eringen's non-local elasticity theory for bending analysis of bi-directional functionally graded Euler-Bernoulli nano-beams", *Int. J. Eng. Sci.*, **106**, 1-9. https://doi.org/10.1016/j.ijengsci.2016.05.005
Nejad, M.Z. and Kashkoli, M.D. (2014), "Time-dependent thermo-creep analysis of rotating FGM thick-walled cylindrical pressure vessels under heat flux", *Int. J. Eng. Sci.*, **82**, 222-237. https://doi.org/10.1016/j.ijengsci.2014.06.006
Nejad, M.Z. and Rahimii, G.H. (2009a), "Elastic analysis of FGM rotating cylindrical pressure vessels", *J. Chin. Inst. Eng.*, **33**(4), 525-530. https://doi.org/10.1080/02533839.2010.9671640
Nejad, M.Z. and Rahimii, G.H. (2009b), "Deformations and stresses in rotating FGM pressurized thick hollow cylinder under thermal load", *Sci. Res. Essays.*, **4**(3), 131-140.
Nejad, M.Z., Rahimii, G.H. and Ghannad, M. (2009), "Set of field equations for thick shell of revolution made of functionally graded materials in curvilinear coordinate system", *Mechanika*, **77**(3), 18-26. https://doi.org/10.5755/j01.mech.77.3.15232
Nejad, M.Z., Rastgoo, A. and Hadi, A. (2014), "Exact elasto-plastic analysis of rotating disks made of functionally graded materials", *Int. J. Eng. Sci.*, **85**, 47-57. https://doi.org/10.1016/j.ijengsci.2014.07.009
Nejad, M.Z., Jabbari, M. and Ghannad, M. (2015a), "Elastic analysis of axially functionally graded rotating thick cylinder with variable thickness under non-uniform arbitrarily pressure loading", *Int. J. Eng. Sci.*, **89**, 86-99. https://doi.org/10.1016/j.ijengsci.2014.12.004
Nejad, M.Z., Jabbari, M. and Ghannad, M. (2015b), "Elastic analysis of FGM rotating thick truncated conical shells with axially-varying properties under non-uniform pressure loading", *Compos. Struct.*, **122**, 561-569. https://doi.org/10.1016/j.compstruct.2014.12.028
Nejad, M.Z., Hoseini, Z., Niknejad, A. and Ghannad, M. (2015c), "Steady-state creep deformations and stresses in FGM rotating thick cylindrical pressure vessels", *J. Mech.*, **31**(1), 1-6. https://doi.org/10.1017/jmech.2014.70
Nejad, M.Z. Hadi, A. and Rastgoo, A. (2016), "Buckling analysis of arbitrary two-directional functionally graded Euler-Bernoulli nano-beams based on nonlocal elasticity theory", *Int. J. Eng. Sci.*, **103**, 1-10. https://doi.org/10.1016/j.ijengsci.2016.03.001
Nejad, M.Z., Hadi, A. and Farajpour, A. (2017a), "Consistent couple-stress theory for free vibration analysis of Euler-Bernoulli nano-beams made of arbitrary bi-directional functionally graded materials", *Struct. Eng. Mech., Int. J.*, **63**(2), 161-169. https://doi.org/10.12989/sem.2017.63.2.161
Nejad, M.Z., Jabbari, M. and Ghannad, M. (2017b), "A general disk form formulation for thermo-elastic analysis of functionally graded thick shells of revolution with arbitrary curvature and variable thickness", *Acta Mech.*, **228**(1), 215-231. https://doi.org/10.1007/s00707-016-1709-z
Nejad, M.Z., Jabbari, M. and Hadi, A. (2017c), "A review of functionally graded thick cylindrical and conical shells", *J. Comput. Appl. Mech.*, **48**(2), 357-370. https://doi.org/10.22059/JCAMECH.2017.247963.220
Nejad, M.Z., Taghizadeh, T., Mehrabadi, S.J. and Herasati, S. (2017d), "Elastic Analysis of Carbon Nanotube-Reinforced Composite Plates with Piezoelectric Layers Using Shear Deformation Theory", *Int. J. Appl. Mech.*, **9**(1), Article Number: 1750011. https://doi.org/10.1142/S1758825117500119
Nejad, M.Z., Alamzadeh, N. and Hadi, A. (2018a), "Thermoelastoplastic analysis of FGM rotating thick cylindrical pressure vessels in linear elastic-fully plastic condition", *Compos. Part B-Eng.*, **154**, 410-422. https://doi.org/10.1016/j.compositesb.2018.09.022
Nejad, M.Z., Hadi, A., Omidvaeri, A. and Rastgoo, A. (2018b),

"Bending analysis of bi-directional functionally graded Euler-Bernoulli nano-beams using integral form of Eringen's non-local elasticity theory", *Struct. Eng. Mech., Int. J.*, **67**(4), 417-425. https://doi.org/10.12989/sem.2018.67.4.417

Robinson, E.L. (1952), "Effect of temperature variation on the long-time rupture strength of steels", *Transaction ASME*, **74**, 777-781.

Samantaray, D., Borah, U., Bhaduri, A. and Dutta, P. (2016), "Effect of semi-solid heat treatment on elevated temperature plasticity of 304L stainless steel", *J. Mater. Sci.*, **51**, 4306-4319. https://doi.org/10.1007/s10853-016-9740-y

Sekkal, M., Fahsi, B., Tounsi, A. and Mahmoud, S.R. (2017), "A novel and simple higher order shear deformation theory for stability and vibration offunctionally graded sandwich plate", *Steel Compos. Struct., Int. J.*, **25**(4), 389-401. https://doi.org/10.12989/scs.2017.25.4.389

Simsek, M. (2016), "Buckling of Timoshenko beams composed of two-dimensional functionally graded material (2D-FGM) having different boundary conditions", *Compos. Struct.*, **149**, 304-314. https://doi.org/10.1016/j.compstruct.2016.04.034

Singh, T. and Gupta, V. (2010), "Modeling steady state creep in functionally graded thick cylinder subjected to internal pressure", *J. Compos. Mater.*, **44**, 1317-1333. https://doi.org/10.1177/0021998309353214

Singh, T. and Gupta, V. (2011), "Effect of anisotropy on steady state creep in functionally graded cylinder", *Compos. Struct.*, **93**, 747-758. https://doi.org/10.1016/j.compstruct.2010.08.005

Singh, T. and Gupta, V. (2012), "Steady-state creep analysis of a functionally graded thick cylinder subjected to internal pressure and thermal gradient", *Int. J. Mater. Res.*, **103**, 1042-1051. https://doi.org/10.3139/146.110738

Singh, T. and Gupta, V. (2014), "Analysis of steady state creep in whisker reinforced functionally graded thick cylinder subjected to internal pressure by considering residual stress", *Mech. Adv. Mater. Struct.*, **21**, 384-392. https://doi.org/10.1080/15376494.2012.697600

Sofiyev, A.H. (2017), "The stability analysis of shear deformable FGM sandwich conical shells under the axial load", *Compos. Struct.*, **176**, 803-811. https://doi.org/10.1016/j.compstruct.2017.06.022

Sofiyev, A.H. (2018a), "Application of the first order shear deformation theory to the solution of free vibration problem for laminated conical shells", *Compos. Struct.*, **188**, 340-346. https://doi.org/10.1016/j.compstruct.2018.01.016

Sofiyev, A.H. (2018b), "Application of the FOSDT to the solution of buckling problem of FGM sandwich conical shells under hydrostatic pressure", *Compos. Part B-Eng.*, **144**, 88-98. https://doi.org/10.1016/j.compositesb.2018.01.025

Sofiyev, A.H. and Osmancelebioglu, E. (2017), "The free vibration of sandwich truncated conical shells containing functionally graded layers within the shear deformation theory", *Compos. Part B-Eng.*, **120**, 197-211. https://doi.org/10.1016/j.compositesb.2017.03.054

Tahami, F.V., Sorkhabi, A.H.D. and Biglari, F.R. (2010), "Creep constitutive equations for cold-drawn 304L stainless steel", *Mat. Sci. Eng: A*, **527**, 4993-4999. https://doi.org/10.1016/j.msea.2010.04.055

Taylor, A., Cizek, P. and Hodgson, P. (2011), "Comparison of 304 stainless steel and Ni–30 wt.% Fe as potential model alloys to study the behaviour of austenite during thermomechanical processing", *Acta Mater.*, **59**, 5832-5844. https://doi.org/10.1016/j.actamat.2011.05.060

Valluri, J.S., Balasubramaniam, K. and Prakash, R.V. (2010), "Creep damage characterization using non-linear ultrasonic techniques", *Acta Mater.*, **58**, 2079-2090. https://doi.org/10.1016/j.actamat.2009.11.050

Viswanathan, R. (1989), *Damage Mechanisms and Life Assessment of High Temperature Components*, ASM International, Ohio, USA.

Wang, Z., Palmer, T.A. and Beese, A.M. (2016), "Effect of processing parameters on microstructure and tensile properties of austenitic stainless steel 304L made by directed energy deposition additive manufacturing", *Acta Mater.*, **110**, 226-235. https://doi.org/10.1016/j.actamat.2016.03.019

Yang, Y. (2000), "Time-dependent stress analysis in functionally graded materials", *Int. J. Sol. Struct.*, **37**, 7593-7608. https://doi.org/10.1016/S0020-7683(99)00310-8

Yao, H.T., Xuan, F.Z., Wang, Z. and Tu, S.T. (2007), "A review of creep analysis and design under multi-axial stress states", *Nucl. Eng. Des.*, **237**, 1969-1986. https://doi.org/10.1016/j.nucengdes.2007.02.003

You, L., Ou, H. and Zheng, Z. (2007), "Creep deformations and stresses in thick-walled cylindrical vessels of functionally graded materials subjected to internal pressure", *Compos. Struct.*, **78**, 285-291. https://doi.org/10.1016/j.compstruct.2005.10.002

CC

Appendix A

$$[B_1]=\begin{bmatrix}0 & 0 & 0 & 0\\ 0 & (1-\upsilon)\dfrac{h^3}{12}R & 0 & 0\\ 0 & 0 & \mu hR & \dfrac{\mu h^3}{12}\\ 0 & 0 & \dfrac{\mu h^3}{12} & \dfrac{\mu h^3}{12}R\end{bmatrix} \tag{A1}$$

$$[B_2]=\begin{bmatrix}0 & (1-\upsilon)\dfrac{h^3}{12} & 0 & 0\\ (1-\upsilon)\dfrac{h^3}{12} & (1-\upsilon)\dfrac{h^2}{12}\left(3R\dfrac{dh}{dx}+h\dfrac{dR}{dx}\right) & -\mu hR & -(\mu-2\upsilon)\dfrac{h^3}{12}\\ 0 & \mu hR & \mu\left(R\dfrac{dh}{dx}+h\dfrac{dR}{dx}\right) & \dfrac{\mu h^2}{4}\dfrac{dh}{dx}\\ 0 & (\mu-2\upsilon)\dfrac{h^3}{12} & \dfrac{\mu h^2}{4}\dfrac{dh}{dx} & \dfrac{\mu h^2}{12}\left(3R\dfrac{dh}{dx}+h\dfrac{dR}{dx}\right)\end{bmatrix} \tag{A2}$$

$$[B_3]=\begin{bmatrix}(1-\upsilon)hR & 0 & \upsilon h & \upsilon hR\\ (1-\upsilon)\dfrac{h^2}{4}\dfrac{dh}{dx} & -\mu hR & 0 & \dfrac{\upsilon h^2}{2}\dfrac{dh}{dx}\\ -\upsilon h & \mu\left(R\dfrac{dh}{dx}+h\dfrac{dR}{dx}\right) & -(1-\upsilon)\alpha & -h+(1-\upsilon)\alpha R\\ -\upsilon hR & \dfrac{\mu h^2}{4}\dfrac{dh}{dx} & -h+(1-\upsilon)\alpha R & -(1-\upsilon)\alpha R^2\end{bmatrix} \tag{A3}$$

$$\{F\}=\frac{1}{E\lambda}\begin{Bmatrix}E\lambda D_1(x)+C_0\\ E\lambda\dfrac{dD_2(x)}{dx}\\ -P\left(R-\dfrac{h}{2}\right)-E\lambda D_3(x)\\ P\dfrac{h}{2}\left(R-\dfrac{h}{2}\right)-E\lambda[D_4(x)+D_5(x)]\end{Bmatrix} \tag{A4}$$

$$\begin{cases}\mu=\dfrac{5}{12}(1-2\upsilon)\\ \alpha=ln\left[\dfrac{\left(R+\frac{h}{2}\right)}{\left(R-\frac{h}{2}\right)}\right]\end{cases} \tag{A5}$$

Also

$$\begin{cases}D_1(x)=R\displaystyle\int_{-\frac{h}{2}}^{\frac{h}{2}}[(1-\upsilon)\varepsilon_x^c+\upsilon(\varepsilon_\theta^c+\varepsilon_z^c)+(1+\upsilon)\alpha_T T]\left(1+\frac{z}{R}\right)dz\\ D_2(x)=R\displaystyle\int_{-\frac{h}{2}}^{\frac{h}{2}}[(1-\upsilon)\varepsilon_x^c+\upsilon(\varepsilon_\theta^c+\varepsilon_z^c)+(1+\upsilon)\alpha_T T]z\left(1+\frac{z}{R}\right)dz\\ D_3(x)=\displaystyle\int_{-\frac{h}{2}}^{\frac{h}{2}}[(1-\upsilon)\varepsilon_\theta^c+\upsilon(\varepsilon_x^c+\varepsilon_z^c)+(1+\upsilon)\alpha_T T]\,dz\\ D_4(x)=\displaystyle\int_{-\frac{h}{2}}^{\frac{h}{2}}[(1-\upsilon)\varepsilon_\theta^c+\upsilon(\varepsilon_x^c+\varepsilon_z^c)+(1+\upsilon)\alpha_T T]\,zdz\\ D_5(x)=R\displaystyle\int_{-\frac{h}{2}}^{\frac{h}{2}}[(1-\upsilon)\varepsilon_z^c+\upsilon(\varepsilon_x^c+\varepsilon_\theta^c)+(1+\upsilon)\alpha_T T]\left(1+\frac{z}{R}\right)dz\end{cases} \tag{A6}$$

Appendix B

$$\{F_c\} = \left\{ E_1(x) + \frac{D_0}{E\lambda} \quad \frac{dE_2(x)}{dx} \quad -E_3(x) \quad -E_4(x) - E_5(x) \right\}^T \tag{B1}$$

$$\begin{cases} E_1(x) = R\int_{-\frac{h}{2}}^{\frac{h}{2}} [(1-\upsilon)\dot{\varepsilon}_x^c + \upsilon(\dot{\varepsilon}_\theta^c + \dot{\varepsilon}_z^c)] \left(1 + \frac{z}{R}\right) dz \\ E_2(x) = R\int_{-\frac{h}{2}}^{\frac{h}{2}} [(1-\upsilon)\dot{\varepsilon}_x^c + \upsilon(\dot{\varepsilon}_\theta^c + \dot{\varepsilon}_z^c)] z \left(1 + \frac{z}{R}\right) dz \\ E_3(x) = \int_{-\frac{h}{2}}^{\frac{h}{2}} [(1-\upsilon)\dot{\varepsilon}_\theta^c + \upsilon(\dot{\varepsilon}_x^c + \dot{\varepsilon}_z^c)]\, dz \\ E_4(x) = \int_{-\frac{h}{2}}^{\frac{h}{2}} [(1-\upsilon)\dot{\varepsilon}_\theta^c + \upsilon(\dot{\varepsilon}_x^c + \dot{\varepsilon}_z^c)]\, z dz \\ E_5(x) = R\int_{-\frac{h}{2}}^{\frac{h}{2}} [(1-\upsilon)\dot{\varepsilon}_z^c + \upsilon(\dot{\varepsilon}_x^c + \dot{\varepsilon}_\theta^c)] \left(1 + \frac{z}{R}\right) dz \end{cases} \tag{B2}$$